ISSN 1674-1056
http://cpb.iphy.ac.cn
http://iopscience.iop.org/cpb
中国物理 B
Chinese Physics
中国物理 Chinese Physics B

Spin Seebeck effect and spin Hall magnetoresistance in the Pt/$Y_3Fe_5O_{12}$ heterostructure under laser-heating

Shuanhu Wang(王拴虎), Gang Li(李刚), Jianyuan Wang(王建元), Yingyi Tian(田颖异), Hongrui Zhang(张洪瑞), Lvkuan Zou(邹吕宽), Jirong Sun(孙继荣), Kexin Jin(金克新)

Citation: Chin. Phys. B . 2018, 27(11): 117201. **doi:** 10.1088/1674-1056/27/11/117201

Journal homepage: http://cpb.iphy.ac.cn; http://iopscience.iop.org/cpb

What follows is a list of articles you may be interested in

Fabrication and characterization of the normally-off N-channel lateral 4H-SiC metal-oxide-semiconductor field-effect transistors

Qing-Wen Song(宋庆文), Xiao-Yan Tang(汤晓燕), Yan-Jing He(何艳静), Guan-Nan Tang(唐冠男),Yue-Hu Wang(王悦湖), Yi-Meng Zhang(张艺蒙), Hui Guo(郭辉), Ren-Xu Jia(贾仁需),Hong-Liang Lv(吕红亮), Yi-Men Zhang(张义门), Yu-Ming Zhang(张玉明)

Chin. Phys. B . 2016, 25(3): 037306. **doi:** 10.1088/1674-1056/25/3/037306

Disorder-enhanced nuclear spin relaxation at Landau level filling factor one

Guan Tong, Benedikt Friess, Li Yong-Qing, Yan Shi-Shen, Vladimir Umansky, Klaus von Klitzing, Jurgen H. Smet

Chin. Phys. B . 2015, 24(6): 067302. **doi:** 10.1088/1674-1056/24/6/067302

Formation of two-dimensional electron gas at AlGaN/GaN heterostructure and the derivation of its sheet density expression

He Xiao-Guang, Zhao De-Gang, Jiang De-Sheng

Chin. Phys. B . 2015, 24(6): 067301. **doi:** 10.1088/1674-1056/24/6/067301

Si and Mg pair-doped interlayers for improving performance of AlGaN/GaN heterostructure field effect transistors grown on Si substrate

Ni Yi-Qiang, He Zhi-Yuan, Yao Yao, Yang Fan, Zhou De-Qiu, Zhou Gui-Lin, Shen Zhen, Zhong Jian, Zheng Yue, Zhang Bai-Jun, Liu Yang

Chin. Phys. B . 2015, 24(5): 057303. **doi:** 10.1088/1674-1056/24/5/057303

Magnetic properties of a Pt/Co_2FeAl/MgO structure with perpendicular magnetic anisotropy

Li Xiao-Qi, Xu Xiao-Guang, Wang Sheng, Wu Yong, Zhang De-Lin, Miao Jun, Jiang Yong

Chin. Phys. B . 2012, 21(10): 107307. **doi:** 10.1088/1674-1056/21/10/107307

SPECIAL TOPIC — 80th Anniversary of Northwestern Polytechnical University (NPU)

Spin Seebeck effect and spin Hall magnetoresistance in the $Pt/Y_3Fe_5O_{12}$ heterostructure under laser-heating*

Shuanhu Wang(王拴虎)[1,†], Gang Li(李刚)[2], Jianyuan Wang(王建元)[1], Yingyi Tian(田颖异)[1], Hongrui Zhang(张洪瑞)[2], Lvkuan Zou(邹吕宽)[3], Jirong Sun(孙继荣)[2], and Kexin Jin(金克新)[1,‡]

[1] *Shaanxi Key Laboratory of Condensed Matter Structures and Properties, School of Science, Northwestern Polytechnical University, Xi'an* 710072, *China*
[2] *Beijing National Laboratory for Condensed Matter and Institute of Physics, Chinese Academy of Sciences, Beijing* 100190, *China*
[3] *High Magnetic Field Laboratory, Chinese Academy of Science, Hefei* 230031, *China*

(Received 21 June 2018; revised manuscript received 25 July 2018; published online 8 October 2018)

In the previous study of longitudinal spin Seebeck effect (LSSE), the thermal gradient was often generated by inserting the sample between the cool bath and the hot bath. For practical use, this method is too cumbersome to be easily integrated into modern electrical circuits. Since the laser can be easily focused into a small region, it will be more convenient and friendly to the integrated circuit. In this paper, we systematically investigate the LSSE and spin Hall magnetoresistance (SMR) of the $Pt/Y_3Fe_5O_{12}$ heterostructure under focused laser-heating. We find that the extremely large voltage of inverse spin Hall effect (V_{ISHE}) can be obtained by reducing the diameter of laser or increasing the number of light spots. Meanwhile, even under the illumination of the ultraviolet light which will excite the electron from the valence band to the conduction band in yttrium iron garnet (YIG), the magnitude of SMR is nearly constant. It indicates that the spin transport behavior of the adjacent Pt is independent of the electron configuration of YIG. The laser-heating method to generate LSSE will be very promising for modern integrated electronic circuits and will promote the application of spin caloritronics in practice.

Keywords: spin Seebeck effect, spin Hall magnetoresistance, laser heating, yttrium iron garnet

PACS: 72.25.Ba, 73.40.–c, 72.10.Di, 75.50.Lk **DOI:** 10.1088/1674-1056/27/11/117201

1. Introduction

Spin current generation has always been an important study of spintronics. The longitudinal spin Seebeck effect (LSSE) has been thought as an effective way to generate the spin current by the thermal gradient. This effect has been observed in a large range of systems, including ferrimagnets,[1–3] antiferromagnetic,[4] and even some paramagnetic materials.[5] Using a metal with strong spin–orbit coupling,[1,6–8] the thermally pumped spin current could be converted to charge current by the inverse spin Hall effect (ISHE). Recently, the conversion of the spin current generated by LSSE to the charge current was also observed in the topological insulator due to the inverse Rashba–Edelstein effect.[9–11] Though there were some disputes about the possible anomalous Nernst effect induced by the magnetized Pt due to the magnetic promixy effect,[12,13] it can be separated by inserting a copper between the yttrium iron garnet (YIG) and Pt,[14] or angle-dependent anisotropic magnetoresistance measurement.[15,16] In addition to the spin Seebeck effect, the spin Hall magnetoresistance (SMR) of Pt/YIG is also observed in the Pt/YIG heterostructure,[17] and it is thought to originate from two processes, namely, the charge current in Pt firstly produces a vertical spin current due to the spin Hall effect (SHE), and then the reflection of this spin current at the Pt/YIG interface generates a charge current that is superimposed on the original one,[18,19] leading to a new kind of magnetoresistance.

In order to generate thermal gradient, the samples are always sandwiched between a resistive heater and a colder bath with thermal sensors mounted on both sides to detect the temperature.[1,20–22] This way of generating a thermal gradient is always too cumbersome and cannot be easily integrated with modern electrical circuits. Recently, Weiler *et al.* found that the focused laser can be used to generate the longitudinal thermal gradient.[23] Kimling *et al.*[24] studied the time-resolved magneto–optic Kerr effect and found the measured time evolution of spin accumulation was on a picosecond time scale, which is too short for contributions from a bulk temperature gradient in YIG. Meanwhile, according to the finite element analysis,[25,26] the laser-induced thermal gradient is mainly located in the illuminated region instead of the whole sample when using the hot-cold bath. Since the laser can be easily focused on the small region, it will be more applicable

*Project supported by the National Natural Science Foundation of China (Grant Nos. 11604265, 51471134, 51572222, and 11704386) and the Fundamental Research Funds for the Central Universities, China (Grant Nos. 3102018zy044 and 3102017jc01001).

†Corresponding author. E-mail: shwang2015@nwpu.edu.cn
‡Corresponding author. E-mail: jinkx@nwpu.edu.cn

© 2018 Chinese Physical Society and IOP Publishing Ltd

to the integrated circuit.[27] However, the systematical investigation on the laser-heating technology is still lacking. Based on this consideration, we carry out a more detailed study on the LSSE and SMR in the Pt/YIG heterostructure under laser-heating, and it is found that the thermal magnons generated by different laser spots do not interfere with each other and they can lineally combine with each other. Therefore, we can separately manipulate the thermal magnons in different regions of YIG by different lasers. We also investigate the SMR of the Pt/YIG heterostructure under the illumination of 360 nm laser. As pointed out in several studies,[15,28,29] the SMR was proposed based on the conversion of charge/spin current under the combined actions of SHE and ISHE near the Pt/YIG interface. Since the photon energy of the ultraviolet laser is above the bandgap of YIG and will excite the electron from the valence band to the conduction band, the question naturally arises as whether the spin transport behavior will be influenced by the variation of electron state of YIG near the interface. Our result shows that the magnitude of SMR presents independence of the ultraviolet laser power, which indicates that the spin transport at the interface of YIG is stable enough even when the electron configuration of YIG near the interface is changed by the ultraviolet illumination. Our research sheds a new light on the application of the spin caloritronics in the electronic industry.

2. Experimental details

The YIG film was first grown above (111)-oriented $Gd_3Ga_5O_{12}$ (5 mm × 3 mm × 0.5 mm) substrate by pulsed laser deposition (PLD) with a thickness of 40 nm which was calibrated by low-angle x-ray. Then Pt with an area of 5 mm × 0.5 mm and a thickness of 5 nm was deposited via the magnetron sputtering, on the top of YIG through a strip-shaped mask. The surface characteristics of YIG were detected by the atomic force microscopy, and the root mean square (RMS) roughness was less than 1.2 Å. Further details on the sample preparation and characterizations can be found in Supplementary material. During the LSSE measurement, the magnetic field (H) was provided by a Helmholtz coil, which could be rotated in the plane of the sample surface. Two electrodes connected to Pt electrode were used to detect the ISHE voltage. The sample was sealed in an electromagnetic shielding box. All the measurement was performed at room temperature. The laser with various wavelengths was focused onto the top of the sample to create a thermal gradient from top to bottom. The laser was mounted on a one-dimensional micro-positioning platform in x direction, as show in Fig. 1(a). The ISHE voltage V_{ISHE} is calculated by $V_{\mathrm{ISHE}} = [V_{\mathrm{ISHE}}(+H) - V_{\mathrm{ISHE}}(-H)]/2$, where $V_{\mathrm{ISHE}}(+H)$ and $V_{\mathrm{ISHE}}(-H)$ are the saturation voltages at magnetic fields pointing to two opposite directions, respectively.

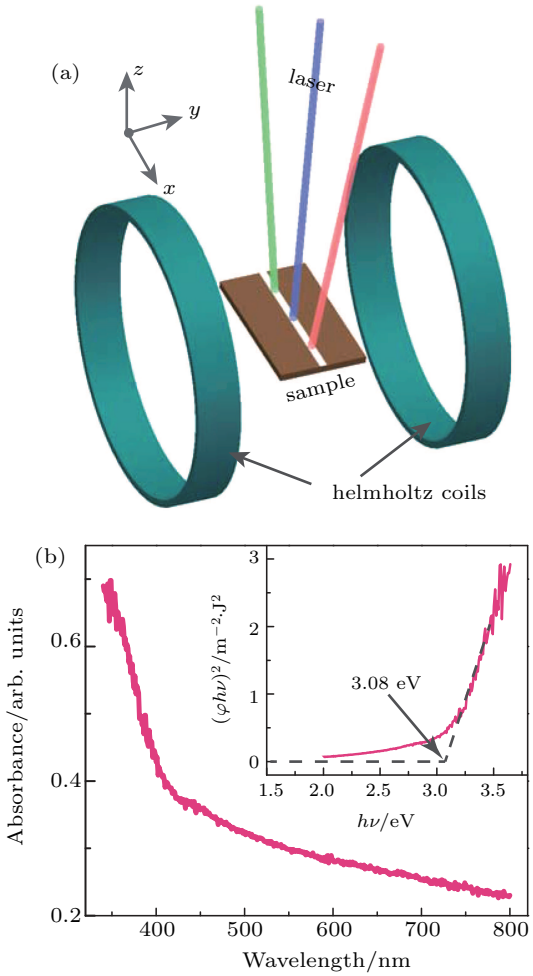


Fig. 1. (color online) (a) The schematic diagram of the experimental setup. (b) The absorbance spectrum of YIG prepared by PLD, and the inset is the corresponding Tauc plot.

3. Results and discussions

The wavelength dependence of the optical absorbance is defined by I_a/I_0, where I_0 and I_a denote the incident and absorbed light intensities, respectively, as shown in Fig. 1(b). According to the absorbance, Tauc plot of $(\varphi h\nu)^2 - h\nu$ shown in the inset of Fig. 1(b) is used to determine the optical bandgap. The absorption coefficient φ is calculated by the equation

$$(I_0 - I_a)/I_a = \exp(-\varphi t), \tag{1}$$

where t is the thickness of 40 nm; h and ν are the Planck constant and the frequency of the light, respectively. By extrapolating the linear portion of the Tauc plot to $\varphi = 0$, we get the band gap of YIG film which is about 3.08 eV, and attribute it to the transition from the O-2p valence band to the Fe-3d conduction band.[30,31]

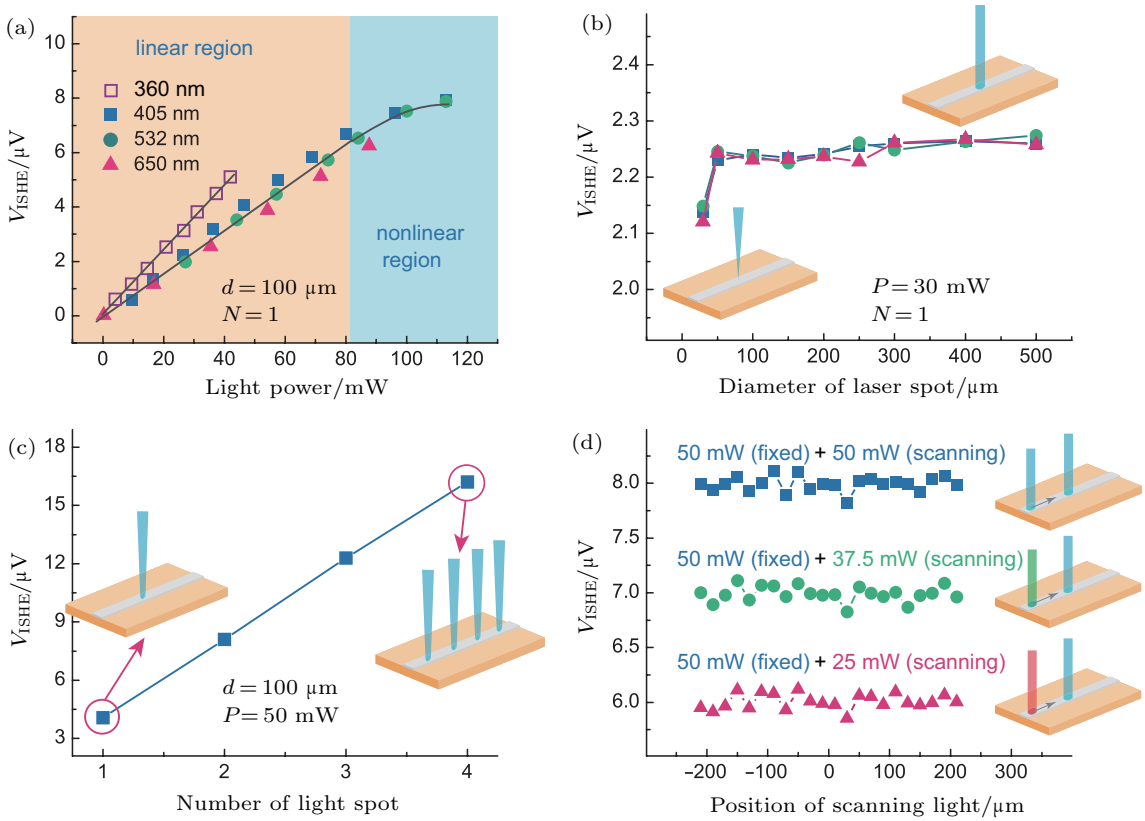


Fig. 2. (color online) V_{ISHE} as a function of (a) the absorbed laser power, (b) the diameter of the light spot, and (c) the number of the light spot, measured with lasers of different wavelengths. The letters P, N, and d denote the light power, the number of the light spot, and the diameter of the laser, respectively. (d) The position dependence of V_{ISHE}. During the measurement, a laser with a wavelength of 405 nm and a power of 50 mW is fixed in the middle of the sample, while another laser with a power of 50 mW, 37.5 mW, and 25 mW, and a wavelength of 405 nm, 532 nm, and 650 nm, is scanning along the Pt electrode, corresponding to the blue, green, and red dots, respectively. The insets are the schematic illustrations of the experiment configuration.

When the laser is focused on the sample surface, YIG will absorb part of the energy. Then an out-of-plane thermal gradient will induce thermal magnons due to LSSE. The spin accumulation will be converted to the charge current in the attached heavy metal due to the ISHE. As shown in Fig. 2(a), the V_{ISHE} firstly increases linearly with the light power below 82 mW due to the increase of the thermal gradient, and then saturates gradually due to the reduction of the magnetization of YIG caused by the increased temperature.[32] The thermal gradient generated by the laser heating is not constant along the direction of the laser. It decays exponentially, and the decay constant depends on the absorption coefficient.[25] As previously reported,[20,33] the average thermal gradient ($\overline{\nabla T}$) is always calculated by dividing the temperature difference by the thickness of the sample, and the temperatures on the top and bottom of the YIG are monitored by the infrared camera (InfReC R500) in this study. The V_{ISHE} versus $\overline{\nabla T}$ curves of different lasers (Fig. S2) coincide with each other, meaning that V_{ISHE} is dependent on the thermal gradient, not the wavelength. However, under the illumination of identical power, the V_{ISHE} generated by 360 nm laser is larger than the one generated by the visible light as shown in Fig. 1(b), which results from the larger thermal gradient induced by larger absorption coefficient of the ultraviolet light.

The detected voltage cannot be ascribed to the so-called photo–spin–voltaic effect. A recent study showed that when the Pt/YIG hybrid structure is exposed to the light, a photon-driven spin-dependent electron excitation will occur near the Pt–YIG interface, producing a photo–spin–voltaic effect.[34,35] Since this effect is independent of the direction of temperature gradient, reversing the direction of thermal gradient will not change its sign. We reversed the incident direction of the light and found a sign change of V_{ISHE} (as shown in Fig. S3).

The magnitude of V_{ISHE} is insensitive to the spot size of the laser, as shown in Fig. 2(b). As the diameter of the laser increases from 20 μm to 500 μm, V_{ISHE} shows a slight increase and remains nearly constant. Remarkably, the magnitude of V_{ISHE} can linearly increase with the number of the light spot. This means that the thermal magnons generated in different regions do not interfere with each other, and they can linearly combine. In the case of four light spots with individual power of 50 mW illuminated simultaneously on YIG, V_{ISHE} can reach as large as 16 μV. Even in this case, the total light spot area is less than 0.15 mm^2. Hence, through reducing the diameter of the laser and increasing the number of spots, the output V_{ISHE} can be increased. This is one of the irreplaceable advantages

of the laser heating technology compared to the hot-cold-bath method. Due to the fact that it is easier to focus laser into a small region, we are able to better control the region of the thermal gradient. The diffusion length of thermal magnons is below 20 μm at room temperature,[25,36,37] and therefore, if the thermal gradient region is 20 μm away from the Pt detector, a minor part of the spin current is converted into the charge current. For the heat-cold-bath method, since the region of the thermal gradient cannot be easily integrated to a small region, the thermal magnon generated 20 μm away from the Pt detector will not contribute to $V_{\rm ISHE}$, thus reducing the efficiency of the thermoelectric conversion. The magnitude of $V_{\rm ISHE}$ is also independent of the laser position if the laser spot is only on the top of the Pt electrode. Setting the middle of the Pt electrode to $x = 0$, we fix a laser with a wavelength of 405 nm and a power of 50 mW at $x = 0$, and collect $V_{\rm ISHE}$ when another laser spot sweeps along the x-axis; we find that the $V_{\rm ISHE}$ keeps nearly constant during the laser spot scanning across the Pt strip, as shown in Fig. 2(d).

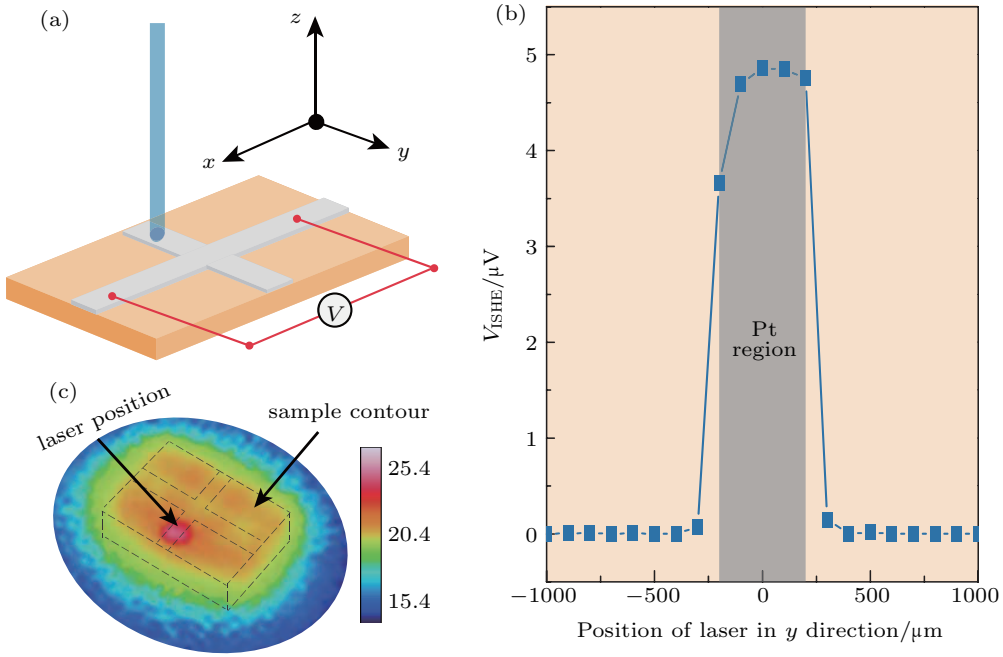


Fig. 3. (color online) $V_{\rm ISHE}$ is measured when the laser is scanning along the transversal Pt. (a) The schematic representation of the experimental geometry. (b) The experimental results. (c) The temperature distribution of the sample surface under the illumination of laser by infrared camera (the dashed lines represent the contour of the sample).

It seems that the Pt layer behaves as a heater and distributes the ∇T uniformly in the YIG, but this is not the case. When the laser is focused on the transversal Pt electrode which is away from the longitudinal Pt, as shown in Fig. 3(a), no detectable voltage is sensed by the nanovoltmeter. Only when the laser is focused on the crossed position of the transversal and longitudinal Pt would we detect the voltage of inverse spin Hall effect, as shown in Fig. 3(b). We also use an infrared camera (InfReC R500) to monitor the temperature distribution of the sample surface under the illumination of laser with a diameter of 0.5 mm. As shown in Fig. 3(c), the temperature is not equally distributed across the sample surface. The heated region is mainly located around the laser spot. Therefore, though the Pt electrode is a metallic layer which always has high thermal conductivity, the thermal gradient is not distributed evenly over YIG by the Pt-layer. It is concluded that regardless of the light wavelength we choose, the $V_{\rm ISHE}$ generated by the two lasers can linearly combine with each other, despite that they are overlapping or separated. Therefore, this technology allows an independent control of thermal magnons by different laser spots.

As shown in Fig. 2(b), the ultraviolet light is more efficient for generating LSSE compared to the visible laser, but the photon energy of 360 nm is quite above the bandgap of YIG as shown by the absorbance spectrum. The higher energy of ultraviolet light will excite the electron from the valence band to the conduction, causing a significant change in the electron configuration of YIG, especially the film near the interface. Since the magnetization is strongly dependent on the electron configuration and the reflection of the spin current is dependent on the magnetization of the ferromagnetic insulator, there are reasons to doubt whether the SMR could be influenced by the ultraviolet. Based on this consideration, the SMR measurement is performed under the illumination of a 360 nm laser (Fig. 4(i)). A current is applied along the x direction and a transversal voltage in y direction is detected in the geometry sketched in Fig. 4(i). A rotating external magnetic field of 500 Oe which is far above the saturation field is

applied and the angle between the field and the current is denoted as α. The YIG sample exhibits low coercivity and the voltage will saturate when the field is increased above 10 Oe, as shown in Fig. S4. Meanwhile, recent studies showed that the LSSE voltage in a Pt/YIG-slab system was suppressed by applying high magnetic fields because of the Zeeman gap in magnon excitation.[38] Therefore, we choose 500 Oe as the magnitude of the external magnetic field. Here the transversal voltage V_y is used to express the SMR effect. This is due to the fact that the transversal resistivity V_y presents a low background signal and thus high signal-to-noise ratio. Meanwhile, $\Delta\rho_{xy}$ is equal to $\Delta\rho_{xx}$ which is evidenced by experiences[32] and theory.[15] The high signal-to-noise ratio helps us get an accurate voltage evolution under the weak light. Otherwise, the weak V_{ISHE} generated by the low power light will be submerged in the background signal.

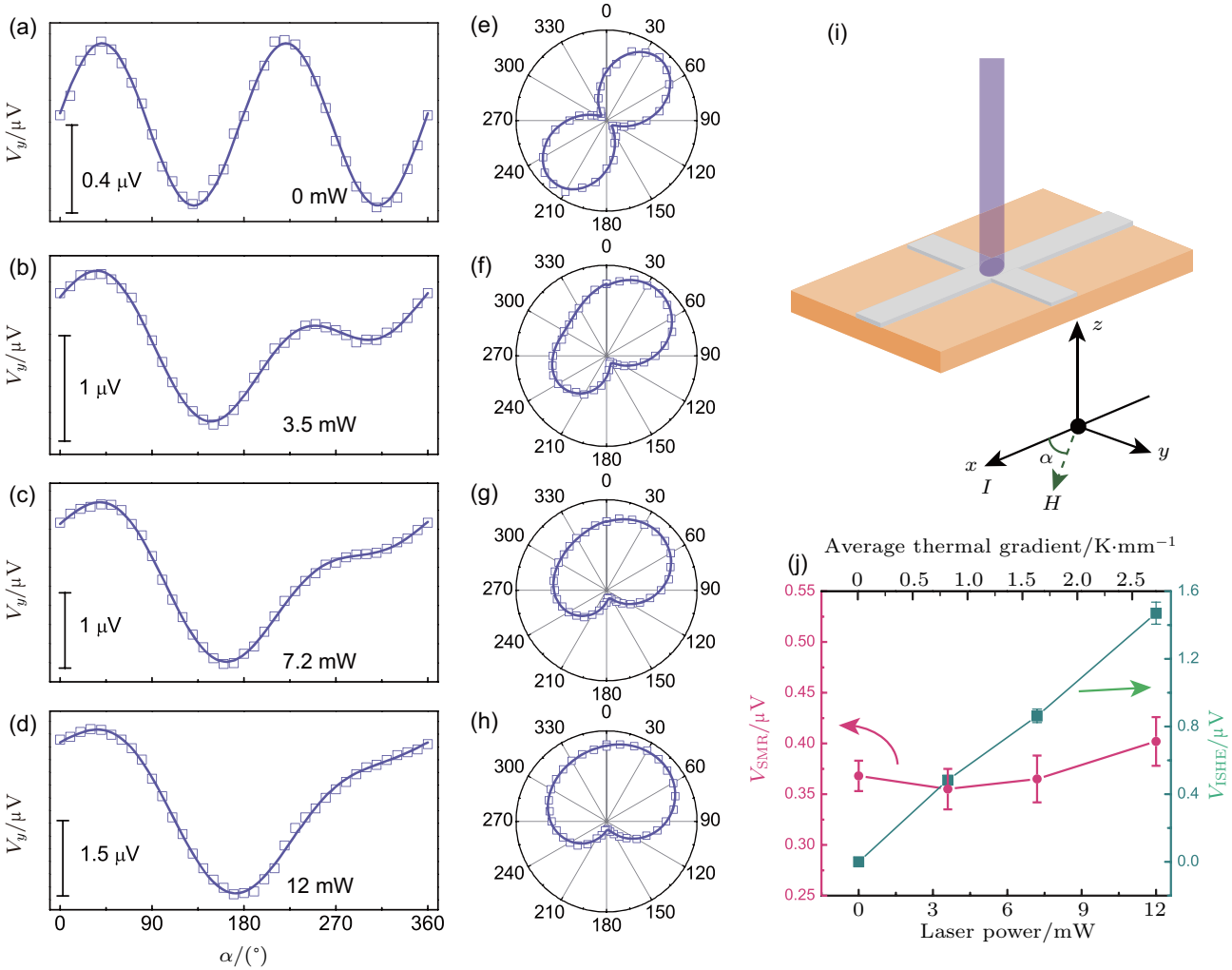


Fig. 4. (color online) Angular dependence of V_y upon illumination of 360 nm laser with a power of (a) 0 mW, (b) 3.5 mW, (c) 7.2 mW, and (d) 12 mW. (e), (f), (g) and (h) show the polar graphs transferred from (a), (b), (c), and (d), respectively. The rotating magnetic field H is 500 Oe. Symbols represent the experimental data and solid lines are the results of curve fitting based on Eq. (2). The current with a magnitude of 50 μA is applied in the x direction, and α is the angle between the applied magnetic field and the current direction, as defined in (i). (j) The laser power dependence of the fitting results of V_{ISHE} and V_{SMR} from Eq. (2).

As shown in Figs. 4(a) and 4(e), without the illumination, the V_y–α relation can be well described by the theory of SMR. To separate the SMR contribution from the anisotropic magnetoresistance due to the proximity effect, the angle-dependent magnetoresistance in which the angle between the charge current and the magnetic field is changed for three different directions is conducted, as shown in Fig. S5, and the results demonstrate that the measured effect is the SMR instead of the AMR. When a weak light with a power of 3.5 mW is focused on the sample, the curve exhibits a complex oscillation, with two unequal maximums and two unequal minimums (Figs. 4(b) and 4(f)). As the power increases, the change of the extreme points becomes more obvious (Figs. 4(c) and 4(g)), which indicates the existence of more than one effect. Due to the different period of voltage with angle, a careful analysis reveals that the V_y–α relation can be well decomposed by

$$V_y = V_{\mathrm{SMR}} \sin(180\alpha) + V_{\mathrm{ISHE}} \cos(360\alpha), \qquad (2)$$

where V_{SMR} and V_{ISHE} are voltages stemming from SMR and ISHE with period of 180° and 360°, respectively. The fitting results agree well with the experimental data. When the power

is increased to 12 mW, the V_{ISHE} has become a principal factor in V_y and the curve changes from the $\sin(180\alpha)$-dominated to the $\cos(360\alpha)$-dominated (Figs. 4(d) and 4(h)). For the laser energy above 12 mW, the SMR signal will be totally submerged in the large LSSE and cannot be separated reliably by the fitting.

According to Eq. (2), we can extract V_{SMR} and V_{ISHE} under the illumination of different powers. As shown in Fig. 4(j), V_{SMR} is nearly constant, indicating that the influence of the electron configuration caused by ultraviolet light on the SMR is not obvious. The V_{ISHE} increases with the laser power and the slope is consistent with previous study without the applied current, as shown in Figs. 2(a) and S2. These results reveal that the two spin-related phenomena, SMR and LSSE, not only do not interfere with each other, but also remain stable even when the electrons in YIG transfer from the valence band to the conduction band. This also provides further evidence that the laser used to generate thermal magnons in YIG will not affect the spin transport behavior in the adjacent Pt.

4. Conclusion

In summary, we systematically investigate the LSSE and SMR under the illumination of ultraviolet and visible light in the Pt/YIG heterostructure. For LSSE, the V_{ISHE} is independent of the size and position of the laser, and thermal magnons generated by different laser spots can linearly combine with each other, meaning that the extremely large V_{ISHE} may be obtained by decreasing the size and increasing the number of lasers. Therefore, the laser-heating technology has substantial advantage over the traditional hot-cold-bath method for future application. Meanwhile, the spin-related phenomenon, SMR, which is thought to be sensitive to the interface of Pt/YIG, is nearly constant even when the electrons transfer from the valence band to the conduction band under the ultraviolet illumination.

Supplementary material

See Supplementary material for the detail of the sample preparation and basic properties, experiments of exclusion of photo–spin–voltaic effect, and angle-dependent magnetoresistance.

References

[1] Uchida K, Adachi H, Ota T, Nakayama H, Maekawa S and Saitoh E 2010 *Appl. Phys. Lett.* **97** 172505

[2] Ramos R, Kikkawa T, Uchida K, Adachi H, Lucas I, Aguirre M H, Algarabel P, Morellón L, Maekawa S, Saitoh E and Ibarra M R 2013 *Appl. Phys. Lett.* **102** 072413

[3] Uchida K i, Nonaka T, Ota T and Saitoh E 2010 *Appl. Phys. Lett.* **97** 262504

[4] Seki S, Ideue T, Kubota M, Kozuka Y, Takagi R, Nakamura M, Kaneko Y, Kawasaki M and Tokura Y 2015 *Phys. Rev. Lett.* **115** 266601

[5] Wu S M, Pearson J E and Bhattacharya A 2015 *Phys. Rev. Lett.* **114** 186602

[6] Uchida K, Ishida M, Kikkawa T, Kirihara A, Murakami T and Saitoh E 2014 *J. Phys.: Condens. Matter* **26** 343202

[7] Magginetti D, Tian K and Tiwari A 2017 *Solid State Commun.* **249** 34

[8] Han F B, Zhang W X, Peng B and Zhang W L 2015 *Acta Phys. Sin.* **64** 247202 (in Chinese)

[9] Mendes J B S, Alves Santos O, Holanda J, Loreto R P, de Araujo C I L, Chang C Z, Moodera J S, Azevedo A and Rezende S M 2017 *Phys. Rev. B* **96** 180415

[10] Boona S R and Heremans J P 2014 *Phys. Rev. B* **90** 064421

[11] Jiang Z, Chang C Z, Masir M R, Tang C, Xu Y, Moodera J S, MacDonald A H and Shi J 2016 *Nat. Commun.* **7** 11458

[12] Huang S Y, Fan X, Qu D, Chen Y P, Wang W G, Wu J, Chen T Y, Xiao J Q and Chien C L 2012 *Phys. Rev. Lett.* **109** 107204

[13] Lu Y M, Cai J W, Huang S Y, Qu D, Miao B F and Chien C L 2013 *Phys. Rev. B* **87** 220409

[14] Kikkawa T, Uchida K, Shiomi Y, Qiu Z, Hou D, Tian D, Nakayama H, Jin X F and Saitoh E 2013 *Phys. Rev. Lett.* **110** 067207

[15] Chen Y T, Takahashi S, Nakayama H, Althammer M, Goennenwein S, Saitoh E and Bauer G 2013 *Phys. Rev. B* **87** 144411

[16] Marmion S R, Ali M, McLaren M, Williams D A and Hickey B J 2014 *Phys. Rev. B* **89** 220404

[17] Nakayama H, Althammer M, Chen Y T, Uchida K, Kajiwara Y, Kikuchi D, Ohtani T, Geprags S, Opel M, Takahashi S, Gross R, Bauer G E, Goennenwein S T and Saitoh E 2013 *Phys. Rev. Lett.* **110** 206601

[18] Li Z D, He P B and Liu W M 2014 *Chin. Phys. B* **23** 117502

[19] Li H N, Hua Z and Li D F 2017 *Chin. Phys. B* **26** 17502

[20] Guo E J, Cramer J, Kehlberger A, Ferguson C A, MacLaren D A, Jakob G and Kläui M 2016 *Phys. Rev. X* **6** 031012

[21] Kehlberger A, Ritzmann U, Hinzke D, Guo E J, Cramer J, Jakob G, Onbasli M C, Kim D H, Ross C A, Jungfleisch M B, Hillebrands B, Nowak U and Klaui M 2015 *Phys. Rev. Lett.* **115** 096602

[22] Ritzmann U, Hinzke D, Kehlberger A, Guo E J, Kläui M and Nowak U 2015 *Phys. Rev. B* **92** 174411

[23] Weiler M, Althammer M, Czeschka F D, Huebl H, Wagner M S, Opel M, Imort I M, Reiss G, Thomas A, Gross R and Goennenwein S T 2012 *Phys. Rev. Lett.* **108** 106602

[24] Kimling J, Choi G M, Brangham J T, Matalla-Wagner T, Huebner T, Kuschel T, Yang F and Cahill D G 2017 *Phys. Rev. Lett.* **118** 057201

[25] An K, Olsson K S, Weathers A, Sullivan S, Chen X, Li X, Marshall L G, Ma X, Klimovich N, Zhou J, Shi L and Li X 2016 *Phys. Rev. Lett.* **117** 107202

[26] Giles B L, Yang Z, Jamison J S and Myers R C 2015 *Phys. Rev. B* **92** 224415

[27] Wang S H, Li G, Guo E J, Zhao Y, Wang J Y, Zou L K, Yan H, Cai J W, Zhang Z T, Wang M, Tian Y Y, Zheng X L, Sun J R and Jin K X 2018 *Phys. Rev. Mater.* **2** 051401

[28] Nakayama H, Althammer M, Chen Y T, Uchida K, Kajiwara Y, Kikuchi D, Ohtani T, Geprags S, Opel M, Takahashi S, Gross R, Bauer G E W, Goennenwein S T B and Saitoh E 2013 *Phys. Rev. Lett.* **110** 206601

[29] Jia X T and Xia K 2011 *Acta Phys. Sin.* **60** 127202 (in Chinese)

[30] Wemple S H, Blank S L, Seman J A and Biolsi W A 1974 *Phys. Rev. B* **9** 2134

[31] Vidyasagar R, Alves Santos O, Holanda J, Cunha R O, Machado F L A, Ribeiro P R T, Rodrigues A R, Mendes J B S, Azevedo A and Rezende S M 2016 *Appl. Phys. Lett.* **109** 122402

[32] Wang S, Zou L, Zhang X, Cai J, Wang S, Shen B and Sun J 2015 *Nanoscale* **7** 17812

[33] Cornelissen L J, Shan J and van Wees B J 2016 *Phys. Rev. B* **94** 180402

[34] Ellsworth D, Lu L, Lan J, Chang H, Li P, Wang Z, Hu J, Johnson B, Bian Y, Xiao J, Wu R and Wu M 2016 *Nat. Phys.* **12** 861

[35] Azevedo A, Cunha R O, Estrada F, Alves Santos O, Mendes J B S, Vilela-Leão L H, Rodríguez-Suárez R L and Rezende S M 2015 *Phys. Rev. B* **92** 024402

[36] Cornelissen L J, Liu J, Duine R A, Youssef J B and van Wees B J 2015 *Nat. Phys.* **11** 1022

[37] Sola A, Bougiatioti P, Kuepferling M, Meier D, Reiss G, Pasquale M, Kuschel T and Basso V 2017 *Sci. Rep.* **7** 46752

[38] Kikkawa T, Uchida K i, Daimon S, Qiu Z, Shiomi Y and Saitoh E 2015 *Phys. Rev. B* **92** 064413